Morphology, thermal, mechanical properties and ageing of nylon 6,6/graphene nanofibers as Nano2 materials

Accepted Manuscript

Morphology, thermal, mechanical properties and ageing of nylon 66/graphene nanofibers as Nano^2 materials

Emanuele Maccaferri, Laura Mazzocchetti, Tiziana Benelli, Andrea Zucchelli, Loris Giorgini

PII: S1359-8368(18)32906-8

DOI: https://doi.org/10.1016/j.compositesb.2018.11.096

Reference: JCOMB 6281

To appear in: *Composites Part B*

Received Date: 6 September 2018

Revised Date: 31 October 2018

Accepted Date: 25 November 2018

Please cite this article as: Maccaferri E, Mazzocchetti L, Benelli T, Zucchelli A, Giorgini L, Morphology, thermal, mechanical properties and ageing of nylon 66/graphene nanofibers as Nano^2 materials, *Composites Part B* (2018), doi: https://doi.org/10.1016/j.compositesb.2018.11.096.

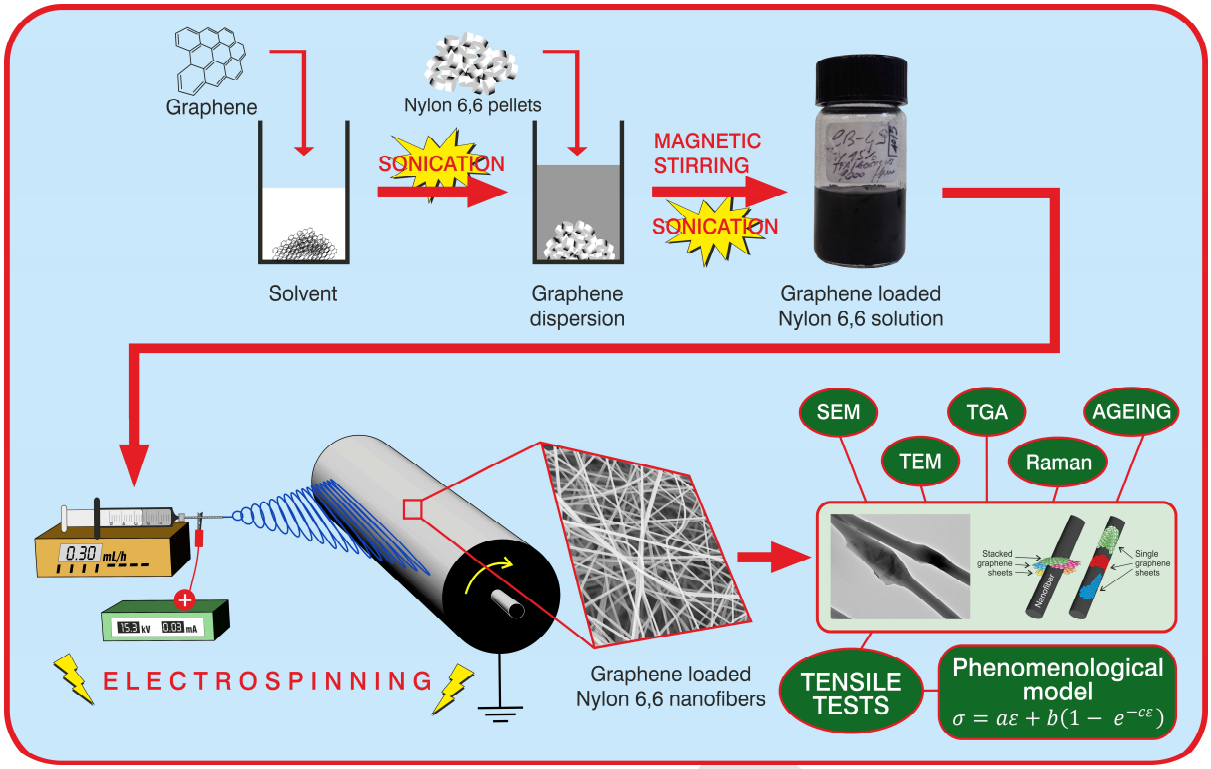

Morphology, Thermal, Mechanical Properties and Ageing of Nylon 66/Graphene Nanofibers as Nano^2 Materials

Emanuele Maccaferri[a], Laura Mazzocchetti[a,b], Tiziana Benelli[a,b], Andrea Zucchelli*[b,c], Loris Giorgini*[a,b]

[a] *Department of Industrial Chemistry "Toso Montanari", University of Bologna, Viale Risorgimento 4, 40136 Bologna, Italy.*

[b] *Interdepartmental Center for Industrial Research on Advanced Applications in Mechanical Engineering and Materials Technology, CIRI-MAM, University of Bologna, Viale Risorgimento 2, 40136 Bologna, Italy.*

[c] *Department of Industrial Engineering, University of Bologna, Viale Risorgimento 2, 40136 Bologna, Italy.*

Abstract: Nylon 66 nanofibers loaded with different Graphene (G) amounts were successfully produced with stable process and good fiber quality, using an optimized solvent system suitable both for electrospinning and for G-suspension. G addition is found to significantly affect diameter but not thermal behaviour. A new phenomenological model is proposed for the interpretation of mechanical behaviour of nanofibrous mat, trying to take into account the nanofibrous morphology. The model highlights a G contribution to mechanical properties that mainly affects the initial steps of deformation where fibers stretch, slide, twist and re-orient. Finally, the nanofibers were analysed after 20 months ageing, showing no significant alteration with respect to the pristine ones, thus the lack of detrimental ageing-effects due to G addition.

Keywords: A. Nano-structures; A. Fibres; A. Polymer-matrix composites (PMCs); B. Thermomechanical; Electrospinning

Authors E-Mails: EM (emanuele.maccaferri3@unibo.it); LM (laura.mazzocchetti@unibo.it); TB (tiziana.benelli@unibo.it); AZ (a.zucchelli@unibo.it); LG (loris.giorgini@unibo.it)

***Corresponding Author**

1. Introduction

Nanoscale reinforcements, such as nanofibers [1], nanoparticles [2] and carbon based nano-reinforcements [3;4], represent a versatile tool for modifying polymer and polymer composite properties. While carbon-based nano-additives may exploit different allotropic forms of C [5;6], Graphene and Related Materials (GRMs), i.e. Graphene (G), Graphene Oxide (GO) and reduced Graphene Oxide (rGO), where carbon atoms are prevalently arranged in two-dimensional monolayer of sp^2 hybridized carbon atoms positioned in a hexagonal lattice [4], are very promising candidates. Although the single graphene sheet is just a few Angstrom thick, the bidimensional layer can easily extend up to hundreds of microns in width; however, it can be reduced to nano-scale dimensions, allowing the creation of the so-called graphene nanoplatelets (GNPs), useful in the preparation of nanocomposites with outstanding properties [7]. In this frame, two-dimensional substrates, not necessarily carbon-based, can also be modified in order to provide additional beneficial properties [5;6;8], without appreciable size and weight penalties [9]. GRMs can be thus effectively used to enhance the mechanical behaviour of polymers. In literature several examples are reported, applying to the widest range of polymeric materials, with gain in both moduli and ultimate properties at break [10-14]. Moreover, thanks to their overall nano-dimensions, GRMs are even suitable for incorporation in polymeric nanofibers, thus creating nanoreinforced nanobjects ($Nano^2$) [15]. Polymeric nanofibers are technologically useful, low-cost, and high surface area materials successfully applied as filtration media, as drug delivery carrier, in tissue engineering as scaffolds for cell growth, they are highly sensitive sensor media and they are reinforcing elements in composites [16;17]. In most cases, nanofibers are themselves used as nano-reinforcements, and the addition of GRMs may be a convenient way to improve the nanofiber properties or to add peculiar properties to nanofibers [18]. It has been indeed proved that nanofibers can positively affect functional and mechanical properties of composites [19] and, when embedded in carbon fiber/epoxy resin composites, the interlaminar fracture toughness and delamination onset fatigue behaviour definitely increase, without a significant impact on the overall dimension of the final composite [16]. While the aspects of the reinforcing effect are still under debate, two main actions are envisaged: the bridging action of the submicrometric filaments keeping together the diverging composites sections and the ability to deviate the crack path, thus enhancing the overall fracture propagation energy [1]. In the field of the delamination toughening, the mechanical performance of the nanofiber membrane plays a crucial role, and Nylon 66 (PA 66) presently represents a popular composite modifier, owing to its low cost, and high melting temperature allowing it to stay in the nanofibrous form during the curing step of many matrices [1]. The improvement of thermal and mechanical behaviour of PA 66 nanofibrous membranes with use of GNPs looks, thus, an attractive perspective for application in composite delamination toughening and many other industrial fields such as, for example, filtration media. Nevertheless it is recognized that evaluation of nanofibrous mats mechanical performances can be tricky, since mechanisms of deformation in non-woven fabrics are based on both fibers and fiber-entanglements

deformations [20], and a correct assessment can be hard to achieve. Indeed, while the greatest part of the literature has been focussed on the evaluation of the nanofibers functional properties, to the best of the Authors' knowledge, only few works [21;22] investigate the mechanical properties of electrospun PA 66 nanofibers reinforced with plain GNPs. Among them, one reports 0.5, 1.0 and 1.5%wt of graphene addition leading to an improvement on both elongation at break and toughness (up to +73% and +50%, respectively), with a concomitant detrimental effect on either Young's modulus or tensile strength (up to –53% and –35%, respectively) of the mat. The second paper accounts for a continuously increasing storage modulus of the fibers with 0.1, 0.5 and 1.0%wt G content: however, in this case fibers are highly aligned and mechanical properties are evaluated only on the basis of DMA measurements; hence no ultimate tensile strength or elongation are investigated. Moreover, no literature at all was found regarding the behaviour of GRMs modified nanofibers upon ageing, in particular when the polymer matrix is crystallizable, such as PA 66. Hence, in the present work PA 66 nanofibers loaded with various amount of graphene are produced and both thermal and mechanical properties are analysed. A broad range of graphene fractions, ranging from very low (500 ppm) to very high (15%wt) content, are considered and investigated. While in many cases graphene based nanocomposite nanofibers are produced thanks to surface modification of carbon nanotubes (CNTs), G or GO, to help the dispersion of the carbonaceous additive [23], one of the purposes of the present work is to provide a simple solvent system for dispersing both the polymer and the graphenic derivative without chemical modification of the latter. In order to obtain graphene loaded electrospun membranes, a solvent system suitable for both suspending graphene and dissolving PA 66 is presented and, for the first time, used for electrospinning purposes. The produced nanofibers are then characterized to determine morphological, thermal and mechanical properties of such membranes, in order to provide a thorough overview of the obtained product. Moreover, the properties of the nanofibrous mats will be investigated both as produced and after 20 months, with the aim of establishing the effects of the carbonaceous additive on the thermal and mechanical properties upon ageing. In this context, a mathematical model has been put forward, to provide help in understanding mechanical behaviour of the electrospun fibers. The model, used to fit the experimental data, would attempt at proposing an easy and simplified interpretation of the complex and multifaceted aspects affecting the mechanical response of a nanofibrous membrane.

2. Materials and methods

2.1 Materials

PA 66 (Nylon 6,6 Zytel E53 NC010 kindly provided by DuPont) was dried in a stove at 110 °C for minimum 6 hours before use. Trifluoroacetic acid (TFA), acetone, 2,2,2-trifluoroethanol (TFE), formic acid and chloroform, all reagent grade, were purchased from Sigma-Aldrich. Solvents were used without further purifications. Graphene nanoplatelets (PURE G+, DirectaPlus) was kindly provided by Reglass s.r.l. - Minerbio (Bologna).

2.2 Preparation of PA 66/Graphene solutions

PA 66 (Nylon 66) solutions (15%wt) were prepared in TFA/acetone 1:1 vol. mixture. Pristine solution was made dissolving PA 66 pellets under magnetic stirring and mild heating (maximum 50 °C) until complete polymer dissolution. Graphene loaded solutions were prepared according to the following method: 1) graphene/solvents mixture sonication via bath sonicator for 30 minutes; 2) graphene/solvents mixture sonication via tip sonicator for 3 hours (instrument settings: amplitude 30%, pulse on 9 s, pulse off 1 s); 3) polymer addition to the graphene dispersion, keeping the mixture under magnetic stirring for minimum 1 hour, and in any case until complete dissolution; 4) mixture sonication via tip sonicator for 4 hours (instrument settings: amplitude 38%, pulse on 9 s, pulse off 1 s). Sonicator bath (type AC 14, Uniset) and tip sonicator (type VCX 750, Sonics, 750W, microtip diameter 3 mm) were used for graphene dispersion. The obtained solutions will be labelled as NY-XG, where X represents the weight fraction of graphene with respect to the polymer in the solution. In **Table S1** the list of the solutions prepared for electrospinning is reported.

2.3 Nanofibrous mats production

Nanofibrous mats were produced via electrospinning technique. A Spinbow® electrospinning machine equipped with four 5 mL syringes was used. Needles (length 55 mm, internal diameter 0.84 mm) were joined to syringes via teflon tubing. Fibers were collected on a rotating drum covered with poly(ethylene)-coated paper at 60 rpm. Mats have final dimensions of approximately 20x40 cm. The obtained nanofibrous mats will be labelled as NanoNY-XG, where X represents the weight fraction of graphene in the electrospun fibers. The electrospinning process was carried out until an average thickness of mat of 50 µm was obtained. In **Table 1** the parameters for optimized electrospinning of nanofibrous mats are reported.

2.4 Characterization of nanofibrous mats

Nanofibrous mats were analysed by scanning electron microscopy (SEM, Phenom ProX) to determine nanofibers morphology. All analysed surfaces were gold coated in order to make them conductive. The distribution of fiber diameters on the electrospun mat was determined through the measurement of approximately 50 fibers by means of an acquisition and image analysis software (ImagePro Plus), and the results were given as the average diameter ± standard deviation. Graphene nanoplatelets dispersion in nanofibers was investigated by transmission electron microscopy TEM: images were acquired by a TEM/STEM FEI Tecnai F20 working at 200 kV. The samples were prepared by direct transfer of fibers on a multifoil-carbon film supported on a copper grid. Raman spectra were recorded with an Ar^+ laser light source (514.5 nm). The Raman spectrometer is also equipped with a Leica DMLM Renishaw 1000 RAMAN Micro-Spectrometer equipped with microscope (objectives 5x, 20x, and 50x), a rejection filter (notch or edge), a monochromator (1200 lines/mm) and a charge-coupled device

thermoelectrically cooled (203 K) detector. DSC measurements were carried out on a TA Instruments Q2000 DSC Modulated apparatus equipped with RCS cooling system. In dynamic runs every sample (5 mg) was heated from 0 °C to 120 °C, cooled to 0 °C, then heated to 290 °C (heating/cooling rate 20 °C) in nitrogen atmosphere.
Tensile tests of selected nanofibrous mats were made using a Instron 5966 universal testing machine equipped with a 100N load cell, speed test 10 mm/min (Supplementary Information S1 for additional details).
Nanofibrous mats for thermal and mechanical properties characterization after 20 months from the production have been kept at ambient conditions without temperature and humidity control.

3. Results and discussion

3.1 Graphene loaded solutions and electrospinning process

Electrospinning needs a homogeneous and process-compatible solution (e.g. acceptable viscosity, sufficient conductivity, adequate solvent system volatility) to be successfully carried out. Graphene loaded solutions, on the other side, require a good stability in terms of time, to guarantee that well exfoliated graphenic sheets do not reaggregate before being interleaved with polymer chains upon polymer solution mixing with GRM suspensions. Hence, the choice of a solvent system which would address both PA 66 solution and graphene suspension is a key factor in the production of high-quality nanofibers.
Formic acid and chloroform/formic acid mixtures are commonly used for dissolving PA 66 in preparation of solutions for electrospinning purposes [24-26]; TFE/formic acid is also a suitable solvent system [27]. A recent work [28] shows the use of TFA/acetone as a good and promising solvent system for the production via solvent casting of GNPs loaded PA 66 films that exhibit smooth surfaces and improved mechanical/electrical properties. Moreover, it is reported that the prepared solutions have good stability in terms of GNPs suspension. Nevertheless, this solvent system has never been used in electrospinning process of PA 66 solutions.
In order to assess the stability of GNPs in different solvent media, several dispersions were produced using the same Nylon 6,6 provided by DuPont and details on the selection of the solvent system are provided in the Supplementary Information (section **S2**). Upon different tests TFA/acetone mixture was proven to lead to the best fibers quality (diameters down to 260 nm, high flow rate up to 0.70 mL/h, absence of beads) and improved electrospinning process stability over the time. Moreover, TFA/acetone 1:1 vol. represents the best solvent ratio: indeed, an increase in the TFA fraction determines an undesired discontinuity in the electrospinning process, while its decrease hampers polymer dissolution (a ratio 3:7 vol. only induces the swelling of PA 66 pellet). The processing conditions should not be able to degrade the polymer; hence no modification of the starting molecular weight is expected. The presence of graphene does not affect significantly the solution electrospinnability, even at

very high graphene concentrations. The electrospinning process is stable, without neither drops expulsion nor needle obstruction, and can be thus positively carried out, once the process parameter optimization has been tailored on the very specific solution characteristics (Table 1). The obtained nanofibrous mats, as reported in Table 1, will be labelled as NanoNY-XG, where X represents the weight fraction of graphene in the electrospun fibers.

3.2 Morphological and structural characterization of electrospun mats

Electrospun nanofibrous mats were assessed via Scanning Electron Microscopy to investigate the morphology and arrangement of the fibers. **Figure 1** displays a panoramic micrograph of the overall membrane aspect, with magnification focussed on the fiber morphology of the different graphene containing formulations produced from the TFA/acetone 1:1 solution. It is clearly observed that fibers do not exhibit any evidence of macroscopic defects, showing instead regular and smooth surfaces. At the highest graphene load values, i.e. 8%wt and 15%wt, and to a smaller extent even at 5%wt and 2%wt, some protrusion can be detected along the fibers, whose presence, however, does not seem to interrupt the seamless fiber continuity. All nanofibers are obtained with a random arrangement, with no significant prevailing orientation neither morphologic defects like beads. While the average diameter of nanofibers stays well below the micrometre threshold, the presence of different graphene loads in the starting solutions affects the fibers' thickness, particularly at low graphene fractions (**Figure 2**).

A clear trend is observed, where a very small amount of graphene, up to 0.1%wt (1,000 ppm), determines a decrease in diameter which lowers the average value of about 40%; a further increase in G percentage causes, instead, the fibers' average size to start increasing again, up to +80% with respect to plain PA 66; +190% with respect to the thinnest 1,000 ppm graphene containing fibers (NanoNY-0.1G). This behaviour could stem from the synthesis of two concomitant phenomena with contrasting effects, namely the raise of both solution conductivity and viscosity induced by the addition of G. Indeed, the first effect favours the stretching of the polymer jet, being the jet itself more sensitive to the electrostatic field; the second, contrarily, hinders the jet stretching, since the presence of G sheets favour chain mobility hinderance hampering the ability of the single chain to untie and elongate. The trend showed in **Figure 2** is therefore explained as such: up to 1,000 ppm of graphene content the raise in conductivity predominates the increment in viscosity, at 2%wt the two effects are perfectly counterbalanced with respect to the plain solution, while for higher G percentages the raise in viscosity is the prevailing result. Nanofibers with low amount of graphene (up to 1.5%wt) have very smooth surfaces; on the contrary, highly graphene loaded nanofibers have less smooth surfaces and the presence of graphene platelets protrusions is detected.

As already pointed out, in SEM images displayed in **Figure 1**, graphene sheets protrusions are clearly observed even at not so high magnification (15,000x), starting from nanofibers with 2%wt of nano-reinforcement (NanoNY-2G). As graphene content increases, nanofibers with high graphene content (NanoNY-8G and NanoNY-15G) not only show lumps caused by the inclusion of wide graphene sheets, but also sudden changes in the single fiber direction linearity, a feature that uncommonly appears in electrospun fibrous membranes. While in principle, the average size distribution of graphene sheets should be the same for all the electrospun solutions, hence expecting thinner diameters to highlight such protruding graphenic sheets far more than thicker ones, this behaviour has not been observed at all up to NanoNY-1.5G. Accurate search of defects in samples up to 1.5%wt G content does not display evidence of defects along the fiber. A TEM investigation of such defects, reported in **Figure 3** for NanoNY-5G and NanoNY-15G, highlights some interesting features. It is worth to point out that the average nanofiber thickness is almost beyond the threshold for electron transparency (200-300 nm), hence the investigation focussed on the thinnest fibers in the mat to allow for the detection of some internal morphology. In **Figure 3A**, the coupling in the same picture of two NanoNY-5G adjacent fibers highlights two significant behaviours: in the upper fiber, the darkening in the colour where the fiber slightly bends and displays some outer protrusion can be associated to some graphenic aggregates coalesced during the processing. This morphological aspect, however, accounts for an almost full inclusion of the carbon-based additive within the fiber boundaries. The lower fiber in **Figure 3A** displays, instead, a bigger lump characterized by wider external lips and by lighter shadows that seem to suggest the stacking of graphenic sheets with concomitant fiber thinning. This observation is confirmed in the TEM micrograph of NanoNY-15G (**Figure 3B**), where a clearly identifiable squared item protrudes out of the fiber, displaying some morphological feature accounting for G sheet stacking, with some wrinkles in the spread platelets. Such piled aggregates might stem from the very high G-concentration in the starting solution and they might be too rigid to bend and comply with the fiber morphology, as it happens, for example, in the upper fiber in **Figure 3A**. The Raman spectrum recorded on the morphologically relevant protruding features (**Figure S4**, in Supplementary Information) is indeed typical of multilayered graphenic sheets [29], with 2D band accounting for at least 5 layers stacking, together with a signal ascribed to the polymeric fiber component. It is worth to point out that Raman spectra recorded on fibers with G content lower than 1.5%wt display only bands typical of the polyamide fraction that reasonably envelops the carbonaceous additive within the fiber boundary (**Figure S4**).

3.3 Thermal characterization of nanofibrous mats

The nanofibrous membranes were investigated via DSC, in order to assess the effect of the carbonaceous nano-additive on the thermal properties of the polymer (**Figure 4**).

All of the investigated samples display, during the first heating scan, an endothermic peak accounting for the melting of the semicrystalline polymer. It is clearly observed that the electrospun PA 66 shows a multiple endotherm centered at T lower than the pellet since, as expected, the processing conditions affect Nylon ability to crystallize with respect to the bulk pellet situation. This behaviour could be related to an average smaller size of the crystallites due to the processing conditions. It has been reported in the literature that molecular orientation and crystallinity of electrospun fibers can be strongly affected by many concomitant factors such as concentration, applied voltage, solvents, polymer molecular properties and others. It has been indeed proved that electrospun PA 66 nanofibers modify their crystallinity depending on the solvent used, (use of Formic acid solution does not lead to any multiple endotherm [30], while Chloroform / Formic Acid 50/50 partially does [31]) as well as on the nanofiber size [30]. This latter parameter is reported to affect also mechanical properties, which are strongly increased below a given diameter, that Baji et al. reported to be lower than 450 nm [30]. Such an effect onto mechanical behaviour however does not infer a concurrent increase in the polymer crystal phase content. In the present case, the average diameter of the obtained nanofiber is at the threshold for a strong contribution of the nanometric dimension of the fibers to the mechanical properties. The addition of graphene to the solution to be electrospun seems to slightly affect the high G-loaded nanofibers (above 2%wt G content in the nanofibers), which display a single melting endotherm, that is however located at a slightly lower T than the PA 66 pellet (**Figure 4**). On the contrary, for smaller ranges of graphene loads (below 2%wt G content in the nanofibers), the electrospinning process seems to highly affect the melting peak with respect to the behaviour of pelletized PA 66, either in the shape and/or in its maximum/maxima position. In particular, the presence of multiple peaks is observed in these cases, with appearance of a higher temperature peak with respect to the corresponding pellet and plain PA 66 (**Figure 4**). It is worth to point out that plain PA 66, with no graphene addition, does not display the peak splitting just upon electrospinning processing. The high T peak appearance, however, has been known for a long time in PA 66 fibers [32] and, even when observed in nanofibers, it is ascribed to the drawing process, where the applied conditions lead to a “more perfect planar zig-zag conformation in the extended chain crystal structures under the influence of applied tensile stress” as found by Gazzano et al. [31], ruling out any difference in the crystal structure [33]. Under the latter assumption, for each sample it has been possible to evaluate the degree of crystallinity (χ_c) of nanofibrous mats according to Equation [1]:

$$\chi_c = (\Delta H_m/\Delta H_{m,100\%}) \cdot 100 \quad [1]$$

where ΔH_m is the melting enthalpy of the sample, $\Delta H_{m,100\%}$ is the melting enthalpy of a hypothetical 100% crystalline PA 66 (196 J/g [34]). ΔH_m used for the calculation refers to the real content of polymer in the nanofiber, thus discarding the graphene presence which does not contribute to the PA 66 crystal melting.

Besides the previously discussed effects of the electrospinning process, thermograms in **Figure 4** and data reported in **Figure 5** display that a graphene content up to 1.5%wt does not affect significantly the nanofibers' degree of crystallinity, which is similar to plain PA 66 nanofibers and pellets. A lower amount of G (NanoNY-0.05G) promotes the high T_m peak without a relevant effect on the overall amount of cristallinity. While it has been reported that G tends to act as a nucleant promoting polymer ability to crystallize, the electrocpinning is known to slighlty hamper the process. Concurrently, it has been reported that smaller diameter nanofibers have usually undergone higher draw ratio, which tends to hamper the formation of bigger and more perfect crystals [30]. The higher nucleating effect of graphene can contrast this behaviour and promote the larger crystal formation. An increase in the graphene content, however, would cause a confinement effect hampering the formation of large crystals. The high T_m peak, indeed, lowers in intensity until it disappears in NanoNY-5G, where the low T_m endothermal transition remains in a position which corresponds to the lower T_m of the nanofibers with low to no graphenic content, and is located at a slightly lower temperature than plain PA 66 pellet, accounting for the presence of smaller and less perfect crystallites. The effect of the higher drawing ratios in the thinnest nanofibers is confirmed also by the slightly higher T_g observed in these samples (**Figure S5** in Supplementary Information).

While the nucleating effect of graphene can be somehow eclipsed by the opposite tendency of thinner nanofiber to hinder crystallization, this feature can be clearly detected in the DSC cooling scans (**Figure 4**). In this case, the nanometric size of the fibers should have been removed upon the first meling, and the nucleating action of graphene promotes crystallization at higher temperature, the higher is the G content. This trend reaches almost a plateau for the highest G loads. The nanofibrous mats thermal behaviour is stable over the time: after 20 months from their production the degree of crystallinity is practically unchanged (dashed bars in **Figure 5**).

3.3 Tensile test of PA 66 nanofibrous mats

While the above discussed thermal features would straightforwardly transfer into modification of the mechanical properties when dealing with bulk materials, the way graphene affects the behaviour of the nanofibrous mats is on the contrary difficult to draw. Selected nanofibrous mats (NanoNY-0G, NanoNY-0.05G, NanoNY-0.1G and NanoNY-1.5G) have been tested to evaluate their mechanical behaviour both as spun and after ageing. The obtained raw results, displayed as load/displacement curves in **Figure S6** in the Supplementary Information, show that in the case of graphene loaded samples the maximum load and the displacement at the maximum load are greater than the plain PA 66 samples. Nevertheless, the corresponding stress-strain curves must be calculated and analysed to provide reliable data to be discussed. The standard approach to deal with mechanical properties is based on the force normalization with respect to the cross-section area, while the displacement is converted in

strain normalizing with respect to the initial length. Using this approach, the cross section of each specimen has been calculated by means of the width and the thickness of mat samples, where the thickness has been estimated with a mechanical micrometre on an area of about 30 mm^2 applying a low preload (100g), in order to reduce the modifications of the mat nanofibrous structure. In **Figure S7** in the supplementary information, examples of the stress-strain curves of "As spun" and "Aged" samples, calculated according to the previous classic approach, are displayed while in **Figure 6** the three main obtained parameters are summarized in bar-chart form: Young's modulus (E), maximum value of stress (σ_{max}) and the strain at which the maximum stress is obtained ($\varepsilon_{\sigma\,max}$). The obtained results show that both E and σ_{max} values are significantly influenced by the graphene content, while $\varepsilon_{\sigma\,max}$ is not. The Young's modulus increases by increasing graphene content and a 50-60% increment (see **Table 2**) can be observed in graphene loaded samples with respect to the pure PA 66, with the maximum increase (61%) in the case of 1,000 ppm of G. Graphene contributes to the σ_{max} (**Table 2**) with increment ranging from 50 to 85% with respect to virgin samples, with the maximum performance obtained in the case of 15,000 ppm G content. Finally, assessment of the aged samples does not highlight a significant change in mechanical performance.

While the above discussed results might well compare with previous literature [21;22] in term of G efficiency in improving mechanical properties, the Authors still had some methodological concern regarding the data analysis and manipulation in the case of nanofibrous specimen: a first topic concerns the stress calculation, while another issue regards the evaluation of the Young's modulus.

Stresses acting on a nanofibrous mat sample under tension are indeed difficult to be exactly calculated because each fiber and the fibers architecture in the mat (fiber orientation, fiber crosses and fiber welds) influence the force distribution in the sample and consequently its mechanical behaviour. The classical approach used in the literature to calculate the stress, based on the evaluation of the cross-section area upon simple measurement of specimen macroscopic width and thickness, is a very rough way to estimate the stress itself. This approach does not account for the fibrous morphology, in particular for fibers' number and diameter and, at the same time, with the previous "classic" approach, the free volume among fibers is wrongly assumed to be filled by the same fiber material as it would be for a bulk object (**Figure 7**). On this point it is worth to point out that the nanofibrous mat porosity, considered as the volume free of polymer over the total volume, can range between 80% and 90% in an average nanofibrous mat. Moreover, whenever a mechanical system is used to estimate the thickness, the measuring system locally perturb the material in a way which is difficult to be evaluated for a sample with at least 80% of void volume. Consequently, the Authors decided to re-analyse experimental raw data (such as **Figure S6**) applying the following Equation [2] that describes the stress as a function of simple and easy to measure quantities [35]:

[2] $$\sigma = \rho \frac{F}{m} L$$

where "m" is the specimen mass (measured in mg), "ρ" is the material density, "L" is the specimen initial length (in mm), F is the force (measured in N) and σ is the stress expressed in MPa. While ρ evaluation should take into account any additive fraction, such as graphene content, in the present case it is assumed to be equal to plain PA 66 density, i.e. 1.14 mg/mm^3, owing to the fact the presence of G would affect the overall values by roughly 1% at the outmost. However, appropriate calculation of such a parameter becomes crucial if a significant additive fraction is used. The idea underlying the proposed formula [2] is that the mass of the sample is redistributed in an ideal sample which has the length of the tested sample but with an ideal cross-section area where there is no free volume between fibers. Based on Equation [2], the tensile test results in terms of force-displacement have been re-calculated; in **Figure S8** in Supplementary Information examples of the new curve are reported and the results obtained applying this new approach are summarized **Figure 8**. It can be noted that values of stress are considerably higher with respect to those calculated with the classic approach, and this fact is due to the evaluation of the equivalent cross-section area calculated by the specimen's mass introduced in Equation [2] that is somehow able to discard the contribution of the voids in the cross-section. Comparing bar charts in **Figure 6A-B** with those in **Figure 8A-B,** it can be pointed out that E and σ_{max} values statistical dispersion is reduced by the implementation of Equation [2] in the calculations. In particular, the average coefficient of variation (defined as the ratio between the standard deviation and the mean value of the data) for Young's modulus and maximum stress calculated with "classic" approach are both around 10%, while, considering the results obtained using Equation [2], the both values drop around 5%. The reduced dispersion on results can be related to the more reliable evaluation of stress based on the latter approach. From a physical point of view, the new analysis procedure confirmed that the ageing did not impact the mechanical behaviour of the materials, while such a new approach supports the idea that graphene just slightly affects $\varepsilon_{\sigma\ max}$ values. The overall trend (**Table 3**) show that NanoNY-0.1G (1,000 ppm G) sample displays the most relevant variation of both E (+59%) and σ_{max} (+55%), with respect to the reference NanoNY-0G. It was indeed previously observed that the best σ_{max} result obtained by classic analysis of data is represented by NanoNY-1.5G (15,000 ppm of G, **Table 2**) while implementation of Equation [2] provides overall results which better agree with the previously discussed data trends on morphology (average diameter, **Figure 2**) and thermal behaviour (degree of crystallinity, **Figure 5**). The discrepancy in the two results can be explained by the different way used to evaluate the stress values: the implementation of Equation [2] in the calculations enables a more realistic evaluation of stress with respect to the application of

cross-section normalization of the Force, where a great amount of the area value is actually composed of voids (**Figure 7**).

Once the concerns regarding a convenient evaluation of the stress have been cleared with the implementation of Equation [2] in the calculations, the issues regarding Young's modulus estimation have been approached. The standard procedure based on the linear regression of the stress-strain data at the early strain stage (from 0.005 mm/mm to 0.015 mm/mm) is considered very well established in literature. Authors, however, would like to highlight that the material stiffness variations described in **Figure S7** and **Figure S8** in Supplementary Information are more complex. In fact, as displayed in **Figure 9**, the material stiffness, calculated as the slope of the tangent to the stress-strain curve, decreases from an initial value down to an asymptotic constant trend. Such a behaviour is peculiar of this type of fibrous materials when they are subjected to tension (see [36-38] where similar stress-strain curves are reported) and it is related to the peculiar nature of the nonwoven structure, which is ascribed to phenomena such as non-homogenous distribution of the fibers, voids, entanglements and twinning of single fibers (bundles). The initial stiffness exhibited by a membrane made of randomly oriented nanofibers subjected to tension, is due to the complexity of fibers network (fibers entanglements, potential adhesion at fibers crosses, fibers bundling, friction between fibers) and to the number of fibers which are aligned along the displacement direction. The initial nonlinear behaviour, with the stiffness lowering, can thus be attributed to the reorganization of fibers in the network, the reduction of intersections and the breaking of those fibers which initially are already under tension. The asymptotic constant trend of the stiffness is the result of the ordered fibers which are, finally, prevalently aligned to the displacement direction. Based on this observation the Authors introduced a new mathematical model for the fitting of the stress-strain experimental results. The model, reported in Equation [3], is considered as the superimposition of two stress contributions, one linear and one nonlinear (σ_1 and σ_2 respectively), as also sketched in **Figure 10A**:

[3] $$\sigma(\varepsilon)=\sigma_1(\varepsilon)-\sigma_2(\varepsilon)=(a\varepsilon+b)-\left(be^{-c\varepsilon}\right)=a\varepsilon+b\left(1-e^{-c\varepsilon}\right)$$

Equation [3] can be used to calculate the slope of the tangent to the stress-strain curve by simple derivation of stress respect strain:

[4] $$\frac{d\sigma}{d\varepsilon}=E(\varepsilon)=a+bce^{-c\varepsilon}$$

where here $E(\varepsilon)$ is used to indicate the function that describes the slope of the tangent and can be interpreted as the local material stiffness or Young's modulus. Using Equation [4] two main features of the model can be obtained:

- the initial material stiffness (or initial Young's modulus, E_0):

[5] $$E_0 = \lim_{\varepsilon \to 0} E(\varepsilon) = a + bc$$

- the asymptotic constant stiffness (or the Young's modulus of the linear trend of stress-strain curve, E_{lin})

[6] $$E_{lin} = \lim_{\varepsilon \to \infty} E(\varepsilon) = a$$

The equations [3], [4] and the particular cases represented by [5] and [6], are all sketched in **Figure 10B**. The model has been used to fit stress-strain results using last square algorithm with excellent results (**Figure S9** in the Supplementary Information), thus allowing to calculate the two main parameters, E_0 and E_{lin}, for both "As spun" and "Aged" specimens (see **Figure 11**). Results obtained by means of model fitting confirm that the ageing does not affect the main material properties. Data obtained using the model fitting previously proposed show that the initial Young's moduli of G modified nanofibrous mats are greater than that of plain PA 66 non-wovens (**Figure 11A**), with NanoNY-0.1G (1,000 ppm) providing the best results. The analysis of the linear portion of the stress-strain curves, represented by the asymptotic constant Young's modulus (E_{lin}), further confirms the benefits provided by integration of G, in particular when in limited amount, showing that in the case of 1,000 ppm G there is an increment, respect to virgin samples, of about 20% of the value. In this frame, the obtained results demonstrate that the presence of G does not alter the linear contribution to the mechanical properties, but, on the contrary, affects the way the nanofibers behave within the complex structure of the mat. Hence there is an initial step where fibers stretch, slide one onto each other, twist and re-orient and this is the parameter which the presence of graphene affects the most: indeed, beside an align increase in the crystalline content of the Nylon, G mainly contributes to the thinning of the spun materials that indeed, keeping constant the volume, produces longer fibers more able to entangle, twist and become interconnected. While these results still confirm the benefits of G addition, the differences highlighted in the G actual effect when switching from the classic method (that well compared with the literature data in terms of extent of the mechanical properties improvements) to the new overall mechanical behaviour approach point out that the nanofiber morphology provides a more challenging substrates for the graphenic additive to express its reinforcing ability at a "bulk material" level. Indeed, the similarity between the size of the nanofibers and of the G sheets dimension (both in the range of few hundreds nanometers) might well be at the limit of an efficient dispersion and interaction of G with polymeric chains for expressing the mechanical reinforcement at its maximum potential (i.e. hindrance of polymer chain mobility, increasing stiffness and strength, preventing cracking, etc).

4. Conclusions

PA 66 nanofibrous mats loaded with different amounts of G were successfully produced with a stable process and good fiber quality, thanks to the optimization of the solvent system. It was then demonstrated that G content strongly affects the fiber diameter in particular at very low amounts of nano-reinforcement. It was also demonstrated that the presence of the carbonaceous additive helps crystal formation, even when the thinning of the fibers and the electrospinning process would hamper it. Moreover, a new phenomenological model has been put forward for the interpretation of the mechanical behaviour of such nanofibrous mats: in this frame a contribution of G has been observed, that affects the initial steps of deformation where fibers stretch, slide one onto each other, twist and re-orient. While this is a preliminary model, whose terms' physical significance is still under investigation, the outstanding fitting performance ability corroborates its significance as a tool for the interpretation of the mechanical behaviour of nanofibrous mats. Finally, the nanofibers were also thermally and mechanically analysed after 20 months ageing, showing no significant alteration with respect to the pristine ones, thus confirming the stability of the process and the lack of detrimental effect in time due to G addition.

Acknowledgements

Authors would like to acknowledge the help of Dr. Juri Belcari for mechanical measurements and Reglass Srl for providing Graphene.

Funding: This work was supported by projects TIME – Integrated Technology for Electric Mobility and ONDA SOLARE funded within POR FESR 2014-2020 action by Regione Emilia Romagna.

Reference List

[1] Palazzetti R, Zucchelli A. Electrospun nanofibers as reinforcement for composite laminates materials - A review. Compos Struct 2017;182(Supplement C):711-27.
[2] Kumar SK, Ganesan V, Riggleman RA. Perspective: Outstanding theoretical questions in polymer-nanoparticle hybrids. J Chem Phys 2017 Jul 11;147(2):020901.
[3] Zhang Y, Rhee KY, Hui D, Park SJ. A critical review of nanodiamond based nanocomposites: Synthesis, properties and applications. Composites Part B 2018;143:19-27.
[4] Papageorgiou DG, Kinloch IA, Young RJ. Mechanical properties of graphene and graphene-based nanocomposites. Prog Mater Sci 2017;90(Supplement C):75-127.
[5] Zhang Y, Choi JR, Park SJ. Thermal conductivity and thermo-physical properties of nanodiamond-attached exfoliated hexagonal boron nitride/epoxy nanocomposites for microelectronics. Composites Part A 2017;101:227-36.
[6] Zhang Y, Rhee KY, Park SJ. Nanodiamond nanocluster-decorated graphene oxide/epoxy nanocomposites with enhanced mechanical behavior and thermal stability. Composites Part B 2017;114:111-20.
[7] Mazzocchetti L, Benelli T, D'Angelo E, Ligi S, Minak G, Poodts E, et al. Managing heat phenomena in epoxy composites production via graphenic derivatives: synthesis, properties and industrial production simulation of graphene and graphene oxide containing composites. 2D Mater 2017;4(1):015020.

[8] Benelli T, Mazzocchetti L, D'Angelo E, Lanzi M, Saraga F, Sambri L, et al. New nitrogen-rich heterocycles for organo-modified bentonites as flame retardant fillers in epoxy resin nanocomposites. Polym Eng Sci 2017 Jun 1;57(6):621-30.
[9] Mazzocchetti L, Benelli T, Maccaferri E, Merighi S, Belcari J, Zucchelli A, et al. Poly-m-aramid electrospun nanofibrous mats as high-performance flame retardants for carbon fiber reinforced composites. Composites Part B 2018;145:252-60.
[10] Vadukumpully S, Paul J, Mahanta N, Valiyaveettil S. Flexible conductive graphene/poly(vinyl chloride) composite thin films with high mechanical strength and thermal stability. Carbon 2011;49(1):198-205.
[11] Istrate OM, Paton KR, Khan U, O'Neill A, Bell AP, Coleman JN. Reinforcement in melt-processed polymer-graphene composites at extremely low graphene loading level. Carbon 2014;78(Supplement C):243-9.
[12] El Achaby M, Arrakhiz FZ, Vaudreuil S, Essassi EM, Qaiss A. Piezoelectric β-polymorph formation and properties enhancement in graphene oxide - PVDF nanocomposite films. Appl Surf Sci 2012;258(19):7668-77.
[13] Kashyap S, Pratihar SK, Behera SK. Strong and ductile graphene oxide reinforced PVA nanocomposites. J Alloy Compd 2016;684(Supplement C):254-60.
[14] Mayoral B, Harkin-Jones E, Noorunnisa Khanam P, AlMaadeed MA, Ouederni M, Hamilton AR, et al. Melt processing and characterisation of polyamide 6/graphene nanoplatelet composites. RSC Adv 2015;5(65):52395-409.
[15] Sisti L, Belcari J, Mazzocchetti L, Totaro G, Vannini M, Giorgini L, et al. Multicomponent reinforcing system for poly(butylene succinate): Composites containing poly(l-lactide) electrospun mats loaded with graphene. Polym Test 2016 Apr;50:283-91.
[16] Brugo TM, Minak G, Zucchelli A, Saghafi H, Fotouhi M. An Investigation on the Fatigue based Delamination of Woven Carbon-epoxy Composite Laminates Reinforced with Polyamide Nanofibers. Procedia Engineering 2015;109(Supplement C):65-72.
[17] Zhang J, Yang T, Lin T, Wang CH. Phase morphology of nanofibre interlayers: Critical factor for toughening carbon/epoxy composites. Compos Sci Technol 2012;72(2):256-62.
[18] Li B, Yuan H, Zhang Y. Transparent PMMA-based nanocomposite using electrospun graphene-incorporated PA-6 nanofibers as the reinforcement. Compos Sci Technol 2013;89(Supplement C):134-41.
[19] An T, Pant B, Kim SY, Park M, Park SJ, Kim HY. Mechanical and optical properties of electrospun nylon-6,6 nanofiber reinforced cyclic butylene terephthalate composites. Journal of Industrial and Engineering Chemistry 2017;55:35-9.
[20] Stanley B, Dewitt RP. Some Principles of Nonwoven Fabrics. Textile Research Journal 1960 Sep 1;30(9):704-11.
[21] Goodarz M, Bahrami SH, Sadighi M, Saber-Samandari S. The influence of graphene reinforced electrospun nano-interlayers on quasi-static indentation behavior of fiber-reinforced epoxy composites. Fibers Polym 2017;18(2):322-33.
[22] Navarro-Pardo F, Martinez-Barrera G, Martinez-Hernandez AL, Castano MV, Rivera-Armenta LJ, Medellin-Rodriguez F, et al. Effects on the Thermo-Mechanical and Crystallinity Properties of Nylon 6,6 Electrospun Fibres Reinforced with One Dimensional (1D) and Two Dimensional (2D) Carbon. Materials 2013;6(8):3494-513.
[23] Navarro-Pardo F, Martinez-Hernandez AL, Velasco-Santos C. Carbon nanotube and graphene based polyamide electrospun nanocomposites: A Review. J Nanomater 2016;2016.
[24] Huang Y, Paul DR. Effect of molecular weight and temperature on physical aging of thin glassy poly(2,6-dimethyl-1,4-phenylene oxide) films. J Polym Sci B Polym Phys 2007 Jun 15;45(12):1390-8.
[25] Liang Y, Zheng G, Han W, Liu C, Chen J, Li Q, et al. Nano-hybrid shish-kebab: Isotactic polypropylene epitaxial growth on electrospun polyamide 66 nanofibers via isothermal crystallization. Mater Lett 2011;65(4):653-6.
[26] Hajiani F, Jeddi AAA, Gharehaghaji AA. An investigation on the effects of twist on geometry of the electrospinning triangle and polyamide 66 nanofiber yarn strength. Fibers Polym 2012;13(2):244-52.
[27] Barkoula NM, Alcock B, Cabrera NO, Peijs T. Fatigue properties of highly oriented polypropylene tapes and all-polypropylene composites. Polym Polym Compos 2008;16(2):101-13.
[28] Papadopoulou EL, Pignatelli F, Marras S, Marini L, Davis A, Athanassiou A, et al. Nylon 6,6/graphene nanoplatelet composite films obtained from a new solvent. RSC Adv 2016;6(8):6823-31.
[29] Ferrari AC, Meyer JC, Scardaci V, Casiraghi C, Lazzeri M, Mauri F, et al. Raman Spectrum of Graphene and Graphene Layers. Phys Rev Lett 2006 Oct 30;97(18):187401.
[30] Baji A, Mai YW, Wong SC. Effect of fiber diameter on the deformation behavior of self-assembled carbon nanotube reinforced electrospun Polyamide 6,6 fibers. Materials Science and Engineering: A 2011;528(21):6565-72.

[31] Gazzano M, Gualandi C, Zucchelli A, Sui T, Korsunsky AM, Reinhard C, et al. Structure-morphology correlation in electrospun fibers of semicrystalline polymers by simultaneous synchrotron SAXS-WAXD. Polymer 2015;63:154-63.
[32] Bell JP, Slade PE, Dumbleton JH. Multiple melting in nylon 66. Journal of Polymer Science Part A2: Polymer Physics 2003 Mar 10;6(10):1773-81.
[33] Hasegawa T, Mikuni T. Higher-order structural analysis of nylon-66 nanofibers prepared by carbon dioxide laser supersonic drawing and exhibiting near-equilibrium melting temperature. J Appl Polym Sci 2014 Mar 16;131(12).
[34] Inoue M. Studies on crystallization of high polymers by differential thermal analysis. J Polym Sci A Gen Pap 1963 Aug 1;1(8):2697-709.
[35] Eskizeybek V, Yar A, Avci A. CNT-PAN hybrid nanofibrous mat interleaved carbon/epoxy laminates with improved Mode I interlaminar fracture toughness. Compos Sci Technol 2018;157:30-9.
[36] Ridruejo A, González C, LLorca J. Micromechanisms of deformation and fracture of polypropylene nonwoven fabrics. Int J Solids Struct 2011;48(1):153-62.
[37] Sinha-Ray S, Yarin AL, Pourdeyhimi B. Meltblown fiber mats and their tensile strength. Polymer 2014;55(16):4241-7.
[38] Molnar K, Vas LM, Czigany T. Determination of tensile strength of electrospun single nanofibers through modeling tensile behavior of the nanofibrous mat. Composites Part B 2012;43(1):15-21.

Table 1 – Electrospinning parameters used for mats production.

Nanofibrous mat	Electrospun solution	Graphene content [(a)] ppm (%wt)	Flow rate mL/h	Electric potential kV	Distance cm	Electric field [(b)] kV/cm	Temperature °C	Relative humidity %
NanoNY-0G	NY-0G	- - -	0.32	20.0	17.0	1.2	26-28	38-40
NanoNY-0.05G	NY-0.05G	500 (0.05)	0.23	20.8	18.0	1.2	26-28	43-45
NanoNY-0.1G	NY-0.1G	1,000 (0.1)	0.25	21.0	18.0	1.2	25-26	54-45
NanoNY-1.5G	NY-1.5G	15,000 (1.5)	0.17	18.0	18.0	1.0	26-27	39-31
NanoNY-2G	NY-2G	20,000 (2.0)	0.50	16.7	15.0	1.1	23-24	33-35
NanoNY-5G	NY-5G	50,000 (5.0)	0.70	17.3	15.0	1.2	24-26	28-30
NanoNY-8G	NY-8G	80,000 (8.0)	0.30	15.1	20.0	0.8	24-26	24-26
NanoNY-15G	NY-15G	150,000 (15.0)	0.50	20.0	15.0	1.3	22-24	31-33

[(a)] referred to the sum of polymer and graphene weights

[(b)] calculated as electric potential to distance ratio

Table 2 – Variation of Young's modulus and maximum value of stress in graphene loaded samples respect to pure PA 66 nanofibrous mat according to evaluation of mechanical properties based on a classic approach.

	Young's modulus (MPa)	**σ_{max} (MPa)**
500ppm VS Virgin	+48%	+50%
1,000ppm VS Virgin	+61%	+57%
15,000ppm VS Virgin	+59%	+85%

Table 3 – Variation of Young's modulus and maximum value of stress in graphene loaded samples respect to pure PA 66 nanofibrous mat based on data analysed with Equation [2].

	Young's modulus (MPa)	**σ_{max} (MPa)**
500ppm VS Virgin	+31%	+32%
1,000ppm VS Virgin	+59%	+55%
15,000ppm VS Virgin	+9%	+43%

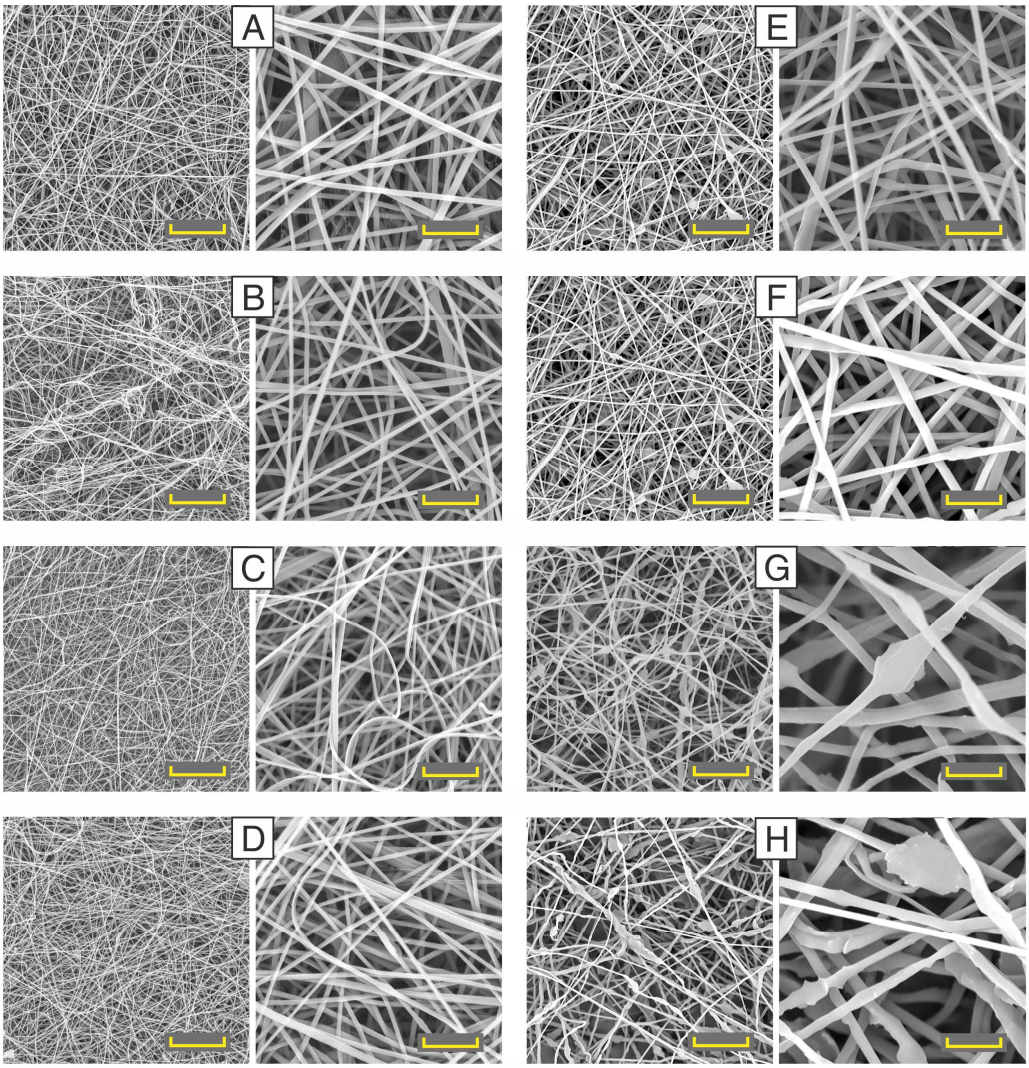

Figure 1 – Electrospun nanofibrous mats at different magnification, left 3000x, right 15000x: (A) NanoNY-0G, (B) NanoNY-0.05G, (C) NanoNY-0.1G, (D) NanoNY-1.5G, (E) NanoNY-2G, (F) NanoNY-5G, (G) NanoNY-8G, (H) NanoNY-15G. Scale bar: left (3000x) 20 µm, right (15000x) 4 µm.

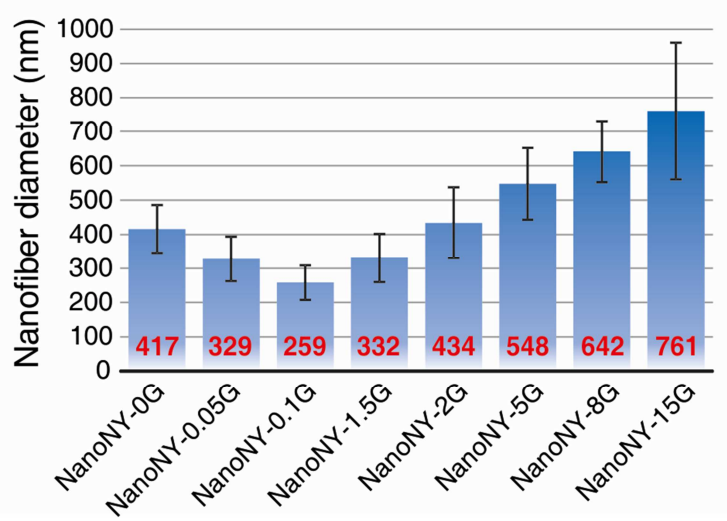

Figure 2 – Nanofiber diameters of produced mats.

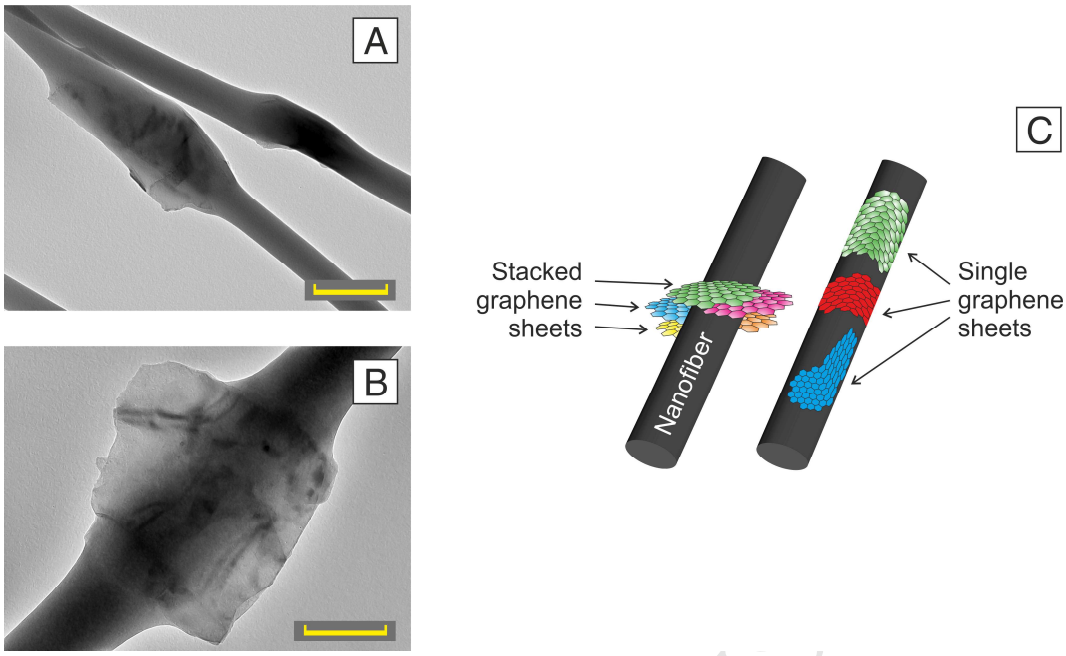

Figure 3 – TEM images of nanofibrous mats loaded with (A) 5%wt of G, scale bar 500 nm, and (B) 15%wt, scale bar 300 nm. (C) Sketch of graphene disposition along the nanofiber.

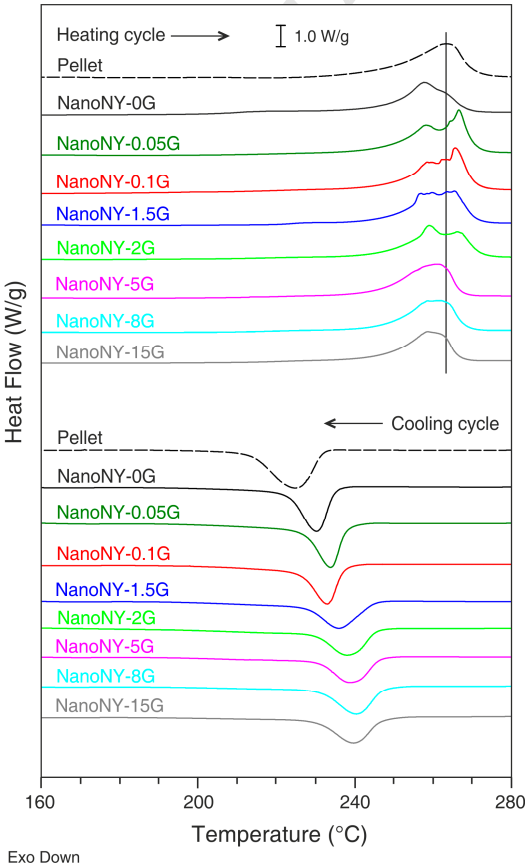

Figure 4 – DSC curves of NanoNY-X mats, heating and cooling scans.

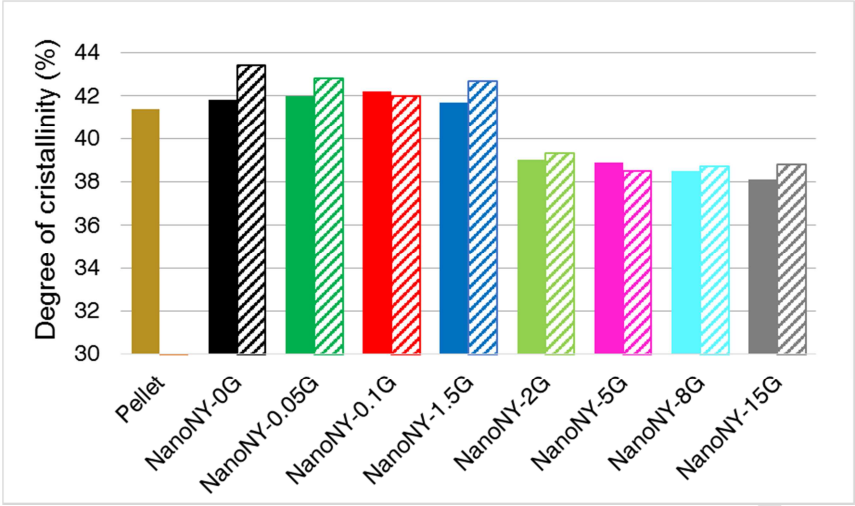

Figure 5 – Degree of crystallinity of PA 66 nanofibrous mats "As spun" (solid bars) and "Aged" (dashed bars) and comparison with PA 66 pellet. Data calculated from DSC curves.

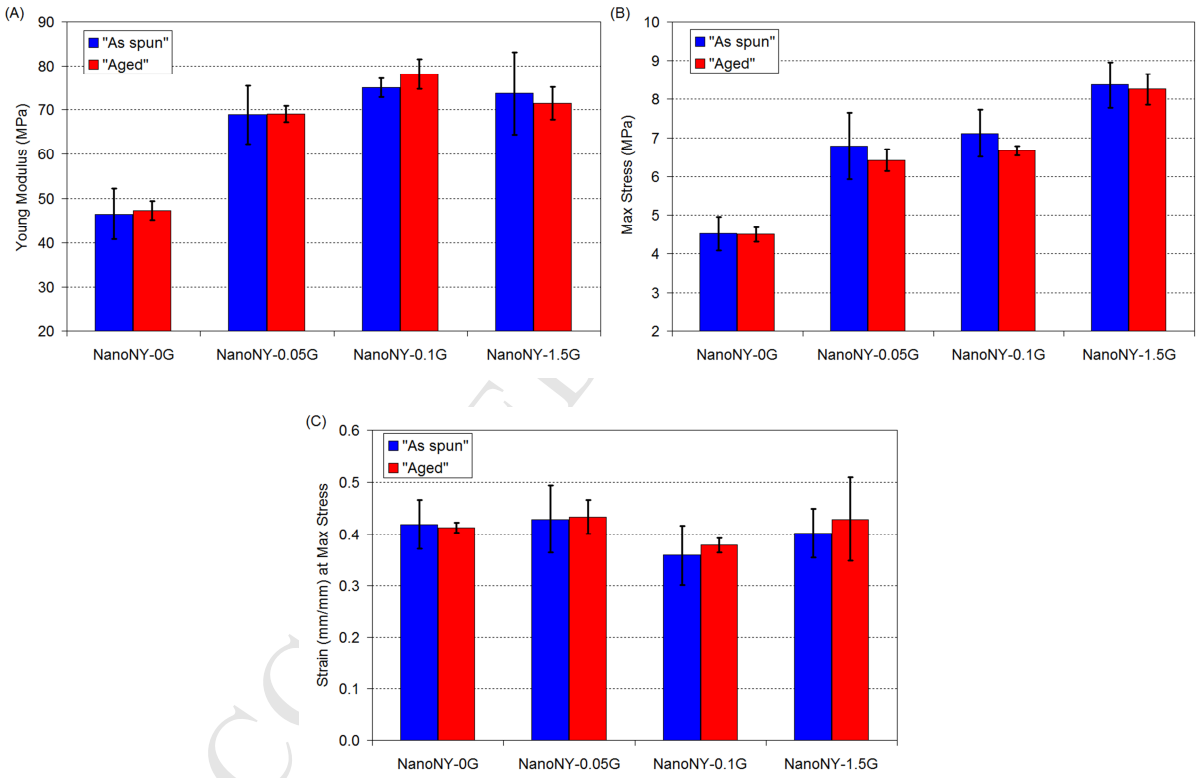

Figure 6 – Results data synthesis according to classic evaluation of the mechanical properties of nanofibrous mats in terms of (A) Young's modulus, (B) maximum stress and (C) strain corresponding to the maximum value of stress.

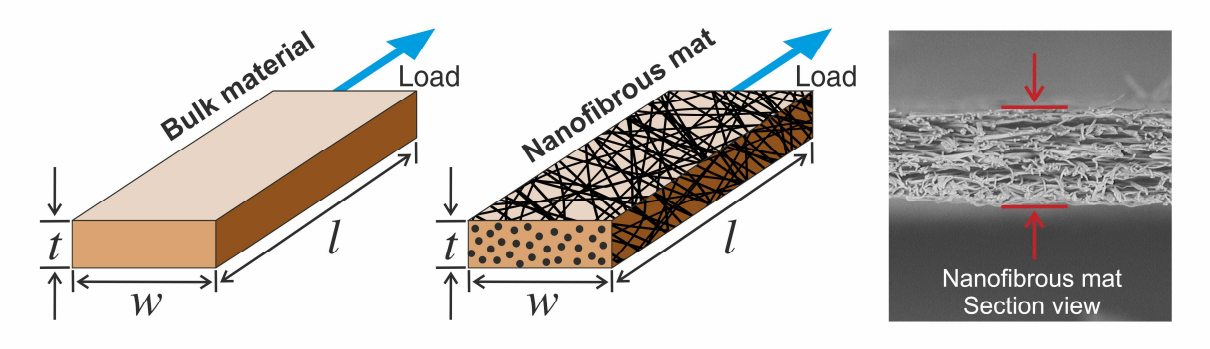

Figure 7 – Schematic representation of bulk versus nanofibrous materials for highlighting the problems in the definition of the cross-section area.

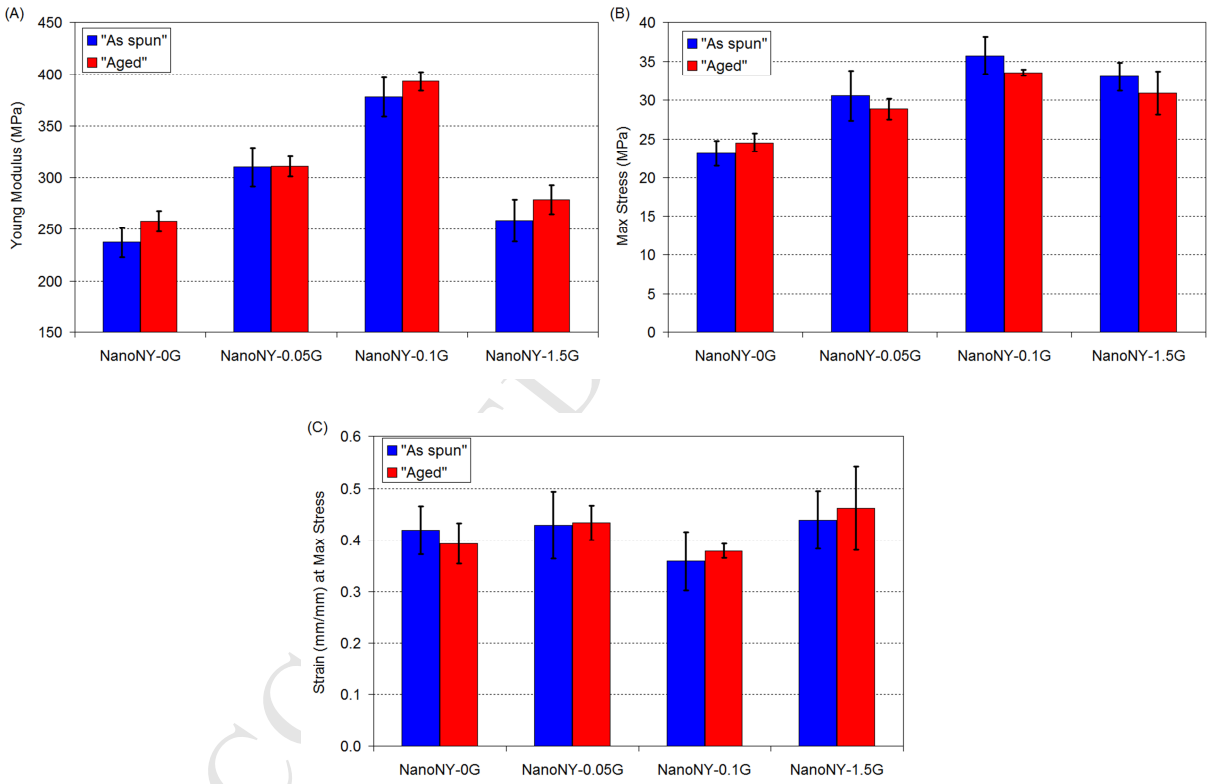

Figure 8 – Results data synthesis from stress calculated by means of equivalent area; (A) Young's modulus, (B) maximum stress and (C) strain corresponding to the maximum value of stress.

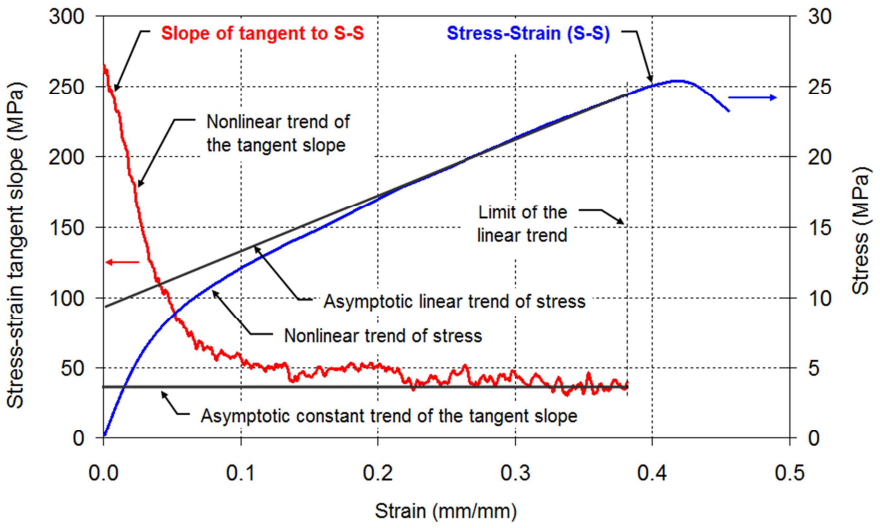

Figure 9 – Example of stress-strain curve (on the right scale) and slope of tangent to stress-strain curve (on the left) where the nonlinear and the asymptotic constant trends are in evidence.

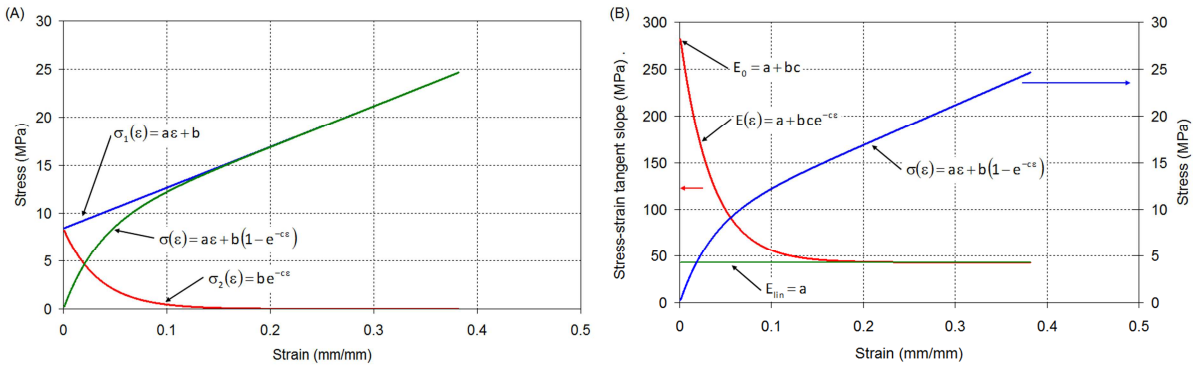

Figure 10 – Graphical sketch (A) of linear (blue) and nonlinear (red) stress terms together with the full model (green) obtained by their combination according to Equation [3], and representation (B) of stress and stiffness mathematical models with the two main parameters E_0 and E_{lin}

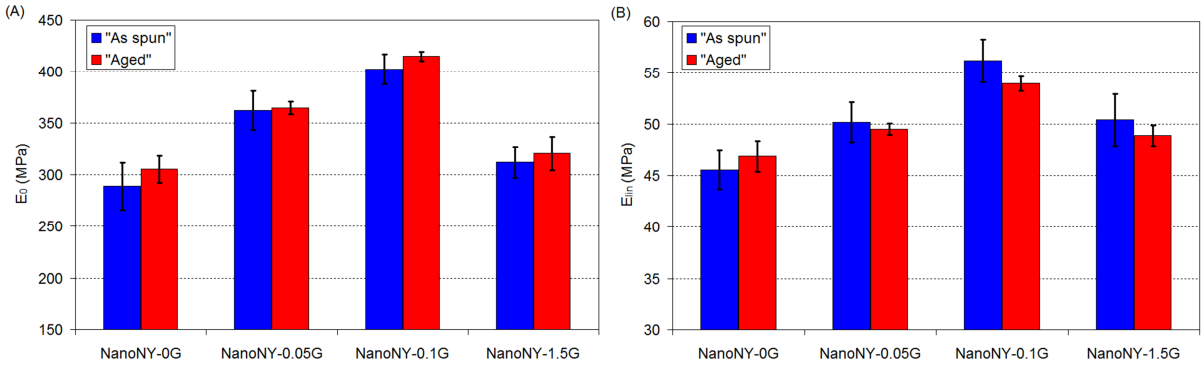

Figure 11 – Bar charts of the initial (A) and of the linear (B) Young's modulus in the case of both "As spun" "Aged" nanofibrous mat.